Contents lists available at ScienceDirect

The Journal of Systems & Software

journal homepage: www.elsevier.com/locate/jss

LWS: A framework for log-based workload simulation in session-based SUT[☆]

Yongqi Han [a], Qingfeng Du [a,*], Jincheng Xu [a], Shengjie Zhao [a], Zhekang Chen [b], Li Cao [b], Kanglin Yin [c], Dan Pei [c]

[a] School of Software Engineering, Tongji University, 201804, Shanghai, China
[b] Bizseer, 100083, Beijing, China
[c] Department of Computer Science and Technology, Tsinghua University, 100084, Beijing, China

ARTICLE INFO

Article history:
Received 3 November 2022
Received in revised form 22 March 2023
Accepted 26 April 2023
Available online 4 May 2023

Keywords:
Workload simulation
Behavior model
Intensity modeling
AIOps

ABSTRACT

Artificial intelligence for IT Operations (AIOps) plays a critical role in operating and managing cloud-native systems and microservice-based applications but is limited by the lack of high-quality datasets with diverse scenarios. Realistic workloads are the premise and basis of generating such AIOps datasets, with the session-based workload being one of the most typical examples. Due to privacy concerns, complexity, variety, and requirements for reasonable intervention, it is difficult to copy or generate such workloads directly, showing the importance of effective and intervenable workload simulation. In this paper, we formulate the task of workload simulation and propose a framework for Log-based Workload Simulation (LWS) in session-based systems. LWS extracts the workload specification including the user behavior abstraction based on agglomerative clustering as well as relational models and the intervenable workload intensity from session logs. Then LWS combines the user behavior abstraction with the workload intensity to generate simulated workloads. The experimental evaluation is performed on an open-source cloud-native application with both well-designed and public real-world workloads, showing that the simulated workload generated by LWS is effective and intervenable, which provides the foundation of generating high-quality AIOps datasets.

1. Introduction

Microservice-based applications composed by loosely coupled services have become the de-facto standard for delivering core business in large IT enterprises due to the independent and scalable nature (Soldani et al., 2018). With the development of cloud computing, microservice-based applications have the promise of migrating to the cloud-native architecture with scalability, resiliency, and elasticity (Kratzke and Quint, 2017). Due to the heterogeneous, asynchronous, and independent nature, artificial intelligence for IT Operations (AIOps) that enhances the quality and reliability of IT service offerings (Notaro et al., 2021) has been proposed and applied in the operation and management of cloud-native systems and microservice-based applications. Despite the steady growing efforts in various AIOps tasks such as anomaly detection and fault localization in recent years, AIOps datasets comprised of execution traces, monitoring metrics, logs, and fault labels commonly suffer from privacy restrictions, scale limitations, few data types and specific scenarios (Li et al., 2022), which makes it difficult to guarantee the generality and real performance of AIOps efforts. Therefore, it is critical to continually generate high-quality AIOps datasets with diverse scenarios for the purpose of assisting and evaluating AIOps researches.

Generating high-quality AIOps datasets requires realistic workloads that represent incoming user requests in specific time intervals as the premise and basis. For commonly treated AIOps tasks such as anomaly detection and fault localization, realistic workloads can produce diverse failure scenarios better than simple constant workloads, which promotes the development of AIOps (Li et al., 2022). One of the most typical workloads is the session-based workload describing the sequence of interdependent requests from the same user in session-based application systems (Goeva-Popstojanova et al., 2006). Generating such workloads in microservice-based applications is not a simple implementation of mocking user operations based on testing tools. Instead, it involves the following major challenges:

(1) The Conflict between Realism and Privacy: Realism in generating workloads is crucial for accurately reflecting real system performance in AIOps datasets. However, for privacy concerns, original real user operations are generally not directly accessible. Instead, observability data such as logs monitoring

[☆] Editor: Jacopo Soldani.
[*] Corresponding author.
E-mail address: du_cloud@tongji.edu.cn (Q. Du).

https://doi.org/10.1016/j.jss.2023.111735
0164-1212/© 2023 Elsevier Inc. All rights reserved.

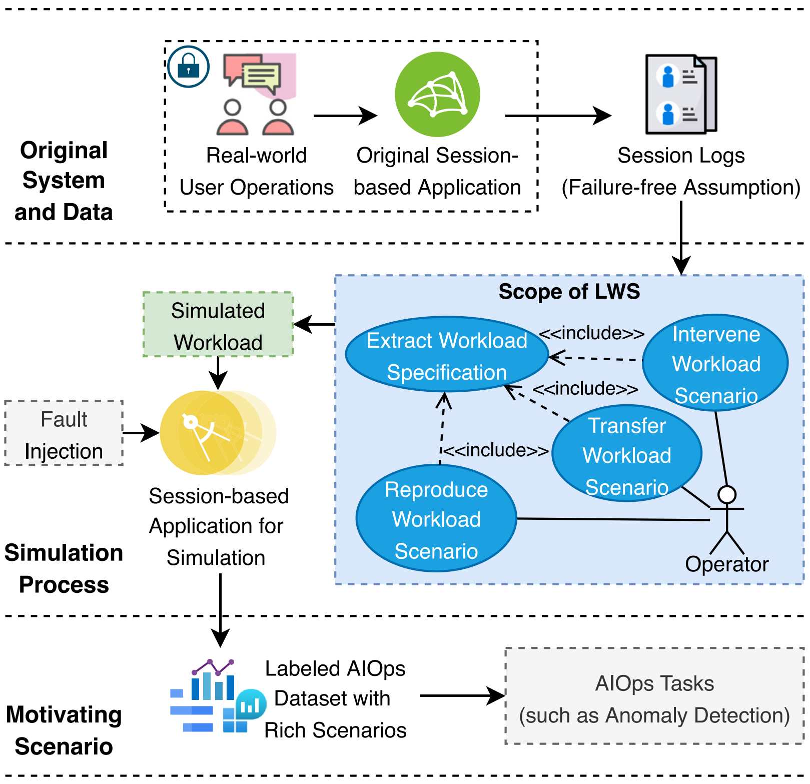
Original System and Data
Real-world User Operations
Original Session-based Application
Session Logs (Failure-free Assumption)
Scope of LWS
Simulated Workload
Extract Workload Specification
<<include>>
Intervene Workload Scenario
Transfer Workload Scenario
Reproduce Workload Scenario
Fault Injection
Session-based Application for Simulation
Operator
Simulation Process
Labeled AIOps Dataset with Rich Scenarios
AIOps Tasks (such as Anomaly Detection)
Motivating Scenario

Fig. 1. The motivating scenario and typical use cases of LWS.

user operations needs to be converted to the workload specification for generation.

(2) Complexity and Variety: Microservice-based applications benefit from the loose coupling characteristic, which enables them to provide more functionalities that can lead to complex user behavior combinations in workloads compared to monolithic applications. Besides, real workloads are usually highly volatile (Reiss et al., 2012), which vary considerably from constant or stepwise increasing workloads usually performed in sandboxed scenarios.

(3) Reasonable Intervention: Some prior knowledge from other similar systems can be referred to in workload generation, such as holidays and events providing somewhat predictable shocks in a wide range of business scenarios (Taylor and Letham, 2018). The reasonable intervention based on prior knowledge in workload generation is beneficial for the analysis of predictable business patterns that happened in similar systems before.

These challenges reflect that the effective and intervenable simulation of workloads for generating AIOps datasets is more suitable and feasible than the simple copy of previous workloads based on original user operations. In response to these challenges, we propose an end-to-end framework for log-based workload simulation (LWS) to extract and generate workloads from logs produced by user operations that happened before in the session-based system under test (SUT). Fig. 1 shows the motivating scenario and typical use cases of LWS. The whole process of AIOps dataset generation and utilization is divided into three parts. First session logs from the original session-based application under real-world user operations are collected as the input of LWS. For potential privacy concerns, LWS is designed to require no additional data from the original system. In consideration of controllability and precise fault labels in AIOps datasets, we separate workloads from faults and assume that all failures in generated datasets are caused by fault injection. Therefore, user behaviors in such session logs are under the failure-free assumption and LWS only considers normal workloads. Then in the simulation process, the workload is simulated by LWS and executes on the session-based application for simulation along with injected faults. The scope of LWS is workload simulation containing typical use cases of reproducing, transferring and intervening workload scenarios as well as extracting workload specification as the basis, differing from the peak or average workload generation in performance testing. Finally, the labeled AIOps dataset with diverse scenarios is generated by collecting observability data in the session-based application for simulation and applied in AIOps tasks such as anomaly detection, which is the motivating scenario of LWS. To meet the above requirements, LWS extracts the workload specification including the user behavior abstraction based on agglomerative clustering as well as relational models and the intervenable workload intensity from session logs. Then LWS combines the user behavior abstraction with the workload intensity to generate simulated workloads. To summarize, the main contributions of our work are as follows:

- We define the task of workload simulation formally with a set of necessary preliminaries. To the best of our knowledge, this is the first formal definition of workload simulation.
- We propose an end-to-end framework named LWS for log-based workload simulation in session-based application systems. LWS extracts the workload specification including the user behavior abstraction and the intervenable workload intensity, combining them for simulated workload generation.
- We perform a case study on an open-source cloud-native microservice demo application with both well-designed and real-world workloads to evaluate LWS comprehensively, demonstrating that LWS can generate effective and intervenable simulated workloads which provide the foundation of generating high-quality AIOps datasets.

2. Related work

The key to workload simulation is the extraction of the workload specification. The workload specification describes key characteristics of user interactions with applications and is commonly summarized and explained by a workload model (Calzarossa et al., 2016). We adopt the division in Vögele et al. (2018) which divides the extraction of the workload specification into user behavior abstraction and workload intensity modeling. We group the related work into the above parts and explain the differences between LWS and existing approaches as follows.

2.1. User behavior abstraction

The user behavior sequence characterizes the single user session including which and how many operations a user finishes per session. One common approach is to configure a fixed sequence of user operations with manual scripts. This approach is simple but hardly varies characteristics and is far from real workloads (Draheim et al., 2006). For more representative user behavior abstraction, approaches based on analysis models are introduced, including approaches based on Markov Chains and Extended Finite State Machines (EFSMs). Markov-Chain-based models assume the memoryless property in the user behavior sequence, which are widely applied in web applications (Li and Tian, 2003). Moreover, Customer Behavior Model Graphs(CBMGs) based on Markov chains which represent classes of users are extracted from logs in different systems (Menascé et al., 1999; Ruffo et al., 2004; Parrott and Carver, 2020). To overcome the limitation of modeling inter-request dependencies (also known as Guards and Actions, GaAs) in Markov-chain-based approaches, Shams et al. Shams et al. (2006) propose an approach relying on EFSMs to describe valid user behavior sequences by predefined state variables as well as GaA parameters. To reduce the number of states in EFSMs, the kTails (Biermann and Feldman, 1972) algorithm which merges pairs of equivalent states is also applied in the process of extraction (Goldstein et al., 2017). WESSBAS (Vögele et al., 2018) combines approaches based on CBMGs and EFSMs, extracts GaAs from production session logs automatically, and generates executable workload models. Schulz et al. (2019) and Barnert and Krcmar (2021) extend WESSBAS to microservice applications and databases by tailoring logs and modifying the Markov chain respectively. Besides, the stochastic form-oriented analysis (Draheim et al., 2006; Lutteroth and Weber, 2008), the probabilistic timed automata (Abbors et al., 2012), the context-based sequential action (Zhou et al., 2014) and the latent features computed by URI space mapping vectors (Erradi et al., 2019) are also applied in user behavior abstraction.

2.2. Workload intensity modeling

As introduced in Curiel and Pont (2018), the workload intensity indicating the number of concurrent users can show daily or weekly access patterns and remarkable increases in short time spans. The constant or stepwise increasing workload intensity is widely used in performance testing frameworks such as Faban[1] and JMeter[2] but cannot describe complex variations of the highly dynamic real-world workload intensity. To define and modify the workload intensity in a flexible and intuitive way, LIMBO (v. Kistowski et al., 2014) allows for modeling and configuring the workload intensity with load profiles and variables describing seasonal patterns, bursts, noise, and monotonic trends. Many approaches focus on workload intensity forecasting. Herbst et al. (2014), Erradi et al. (2019), Fei et al. (2020), Feng et al. (2022) forecast the workload intensity by choosing suitable regression models including the Elastic Net regression model, the boosting decision tree regression prediction model, the Ridge regression model, the Lasso regression model, and the Multi-Layer Perceptron. Time series forecasting approaches including Telescope and Prophet are also applied to forecast the context-tailored workload intensity (Schulz et al., 2021). Besides, there also exist approaches replaying the workload directly (Fattah et al., 2020).

2.3. Differences between LWS and existing approaches

Most existing approaches only focus on workload specification extraction and the replay of original workloads. WESSBAS (Vögele et al., 2018) which extracts the relational model from HTTP request logs, generates the workload intensity based on LIMBO (v. Kistowski et al., 2014) and uses a domain-specific language (DSL) to specify workload models is a classic example and similar to our approach. Compared with these approaches, LWS has a fundamentally different goal of reproducing, transferring, and intervening workload scenarios for generating high-quality AIOps datasets with diverse scenarios rather than mere performance testing. Therefore, LWS focuses on quick, extensible, and intervenable workload generation instead of the peak or average workloads commonly used in WESSBAS and other approaches. As introduced in Section 4, LWS refers to the automatic GaA extraction process of WESSBAS in user behavior abstraction but abstracts the user behavior by a more general method and Hierarchical clustering. Moreover, LWS explores different strategies of workload intensity modeling and combines them for workload simulation which can be intervened effectively for quick, extensible, and intervenable workload generation. Besides, some other approaches (Herbst et al., 2014; Erradi et al., 2019; Fei et al., 2020; Schulz et al., 2021; Feng et al., 2022) attempt to forecast future workloads based on time series forecasting and workload specification. Different from these approaches, LWS provides an e2e framework for workload simulation rather than specific forecasts for concrete systems.

3. Problem definition

In this section, we present a set of formal descriptions for the task of workload simulation. First, we introduce the definition of user behaviors.

Definition 1 (*User Behavior*)**.** *Let $\mathcal{T}$ be a session-based SUT. A user behavior (denoted by u) is a single logical unit of work executed by the end user, which can access and possibly modify the contents in $\mathcal{T}$.*

A session is a series of contiguous actions by a user on an individual system within a given time frame that is stored on the server side, but which action is a user behavior u for workload simulation? To guarantee that u can be properly selected, we propose the ASID properties. We do not claim these properties to be a complete set of desiderata, but they can be seen as a good starting point toward the understanding of u in workload simulation.

(1) Atomicity: The entire u takes place at once or does not happen at all. It will not occur partially. For example, an HTTP request can only be sent to $\mathcal{T}$ or not, and there is no midway. Hence, an HTTP request follows atomicity. On the contrary, a sequence of HTTP requests can be executed one by one in the beginning and not be executed anymore for the rest. Hence, a sequence of HTTP requests disobeys atomicity, and cannot be seen as the user behavior. The atomicity property helps to determine the granularity of u.

[1] http://faban.org/
[2] https://jmeter.apache.org/

(2) Security: The user behavior u must not result in the failure of $\mathcal{T}$. For example, if a request leading to SQL injection attacks can crash the database, then $\mathcal{T}$ will not be able to process the subsequent requests normally. The security property makes sure that $\mathcal{T}$ can always process the user behaviors in the original and simulated workload.

(3) Isolation: Multiple user behaviors can occur concurrently without leading to the inconsistency of the state of $\mathcal{T}$. Changes occurring in a particular u will not be visible to any other u until the particular change is written to memory or has been committed. Usually, the isolation property is provided by $\mathcal{T}$ for all the received requests.

(4) Durability: Once a user behavior u has completed execution, updates and modifications to $\mathcal{T}$ are stored and persist even if a system failure occurs. For example, the mouse-move event is usually meaningless for the system state and will not be stored by $\mathcal{T}$. Even though it is a necessary action executed by the user, it should not be seen as a user behavior. The durability property helps to exclude insignificant actions and focus on key user behaviors.

In a web-based application $\mathcal{T}$, a single HTTP request satisfying the ASID properties can be seen as a user behavior u. According to the request URL and the request method (GET/POST), user behaviors can be further divided into different types. We assume that parameters and their values do not affect the taxonomy of u in this paper. Based on the definition of user behaviors, we define the user behavior sequence as follows:

Definition 2 (*User Behavior Sequence*)**.** *Let $\mathcal{T}$ be a session-based SUT and u_i be the ith user behavior within a session. A user behavior sequence denoted by S is an ordered sequence of $(u_1, u_2, \cdots, u_l)$ which can be executed entirely without raising errors in $\mathcal{T}$.*

Consider the following case. Assume that u_a is the user behavior of "add_to_cart" and u_b is "placing_order". The SUT $\mathcal{T}$ requires that u_b cannot be executed alone and u_a must always precede u_b. If we try to execute an ordered sequence of (u_b, u_a) forcefully, then the sequence is definitely illegal and it may even lead to a system crash in $\mathcal{T}$. Hence, if a sequence could raise an error, we do not treat it as a user behavior sequence S.

In a web-based application $\mathcal{T}$ where a single HTTP request is u, S can be seen as an ordered sequence of HTTP requests within a session. For simplicity, we refer to a user behavior sequence as a session, and we use both terms throughout the rest of the paper.

In workload simulation, what to do is important, and it has been guaranteed by S as the action dimension. On the other hand, when to do is also important. The definition of workload intensity provides the time dimension:

Definition 3 (*Workload Intensity*)**.** *Let $I : t \to N^+$ be the function returning the number of active sessions at the timestamp of t. The workload intensity, denoted as I, is a sequence of discrete-time data indexed in time order whose y-value is $I(t)$.*

In a real system, the number of active sessions is usually collected by the monitoring facilities with unceasing regularity, for example, every 15 seconds. Hence, we define x-value t of the workload intensity I on a discrete domain rather than a continuous domain.

Now we present the definition of workload simulation.

Definition 4 (*Workload Simulation*)**.** *Given a series of user behavior sequences $\Omega(S) = \{S_1, \cdots, S_k\}$ and the workload intensity I, $\Omega(S)$ will be executed on the session-based SUT $\mathcal{T}$ scheduled by I to produce the original workload, and a set of logs will be collected. Workload simulation aims to produce a new workload containing characteristics of the original workload and reasonable interventions from existing real workload patterns.*

It is worth mentioning that the task of workload simulation is not to achieve a 1:1 emulation of the original workload or just workload execution. On the one hand, a specific user behavior sequence S is meaningless in a workload containing thousands of sessions. We are more interested in how a group of users interact with $\mathcal{T}$ rather than how a specific user interacts with $\mathcal{T}$. On the other hand, workload simulation is not the final purpose but a compulsory task for generating high-quality AIOps datasets with diverse scenarios. We may want to increase the number of users, improve the architecture of SUT or transfer the workload to a new environment. User behavior abstraction and workload intensity modeling will be more helpful.

More concretely, the simulated workload should be similar to the original workload in terms of user behaviors and the workload intensity while keeping $\mathcal{T}$ the same. Moreover, performance metrics collected by monitoring facilities should also keep similar between the original workload and the simulated workload.

4. LWS framework

In this section, we zoom in on the details of our proposed LWS framework. The architecture has been illustrated in Fig. 2, which consists of four different components:

- **Log Collection and Transformation:** Collect and pre-process logs from the SUT under the original workload.
- **User Behavior Abstraction:** Infer a high-level representation from thousands of sessions to describe user behaviors in a probabilistic way.
- **Workload Intensity Modeling:** Describe the number of active sessions indicating concurrent users as a time series for workload simulation.
- **Simulated Workload Generation:** Generate executable workloads based on user behavior abstraction and workload intensity.

4.1. Log collection and transformation

A wide variety of monitoring facilities can be used for log collection. According to the deployment architecture of $\mathcal{T}$, developers or testers can take suitable solutions to monitor the original workload (as well as the simulated workload), especially in the cloud-native systems integrating with observability specifications such as OpenTelemetry[3] and tools such as Filebeat[4] and Elasticsearch[5] naturally.

A system can generate hundreds of logs in very little time, but not all the collected logs are necessary for workload simulation such as standalone logs recording event messages from the operating system. According to the definition of workload simulation, $\Omega(S) = \{S_0, \cdots, S_k\}$ and I provide the action dimension and the time dimension as the necessary conditions. Therefore, the request-related logs to be filtered out are expected to contain the unique identifier to indicate a session (e.g., session ID), the request starting time, the request path, and the request parameters in a session-based application.

After the logs have been collected and filtered, we need to alter the structure and format of raw data to make it better organized for the analysis of the original workload. The useless fields will be removed to save storage space and reduce useless calculations. Under multiple concurrent requests, the collected logs are usually out of order, so we need to group them by the unique identifier and sort the logs by the request start time within each session. Now, the pre-processed logs are ready for the next steps.

3 https://opentelemetry.io/
4 https://github.com/elastic/beats
5 https://github.com/elastic/elasticsearch

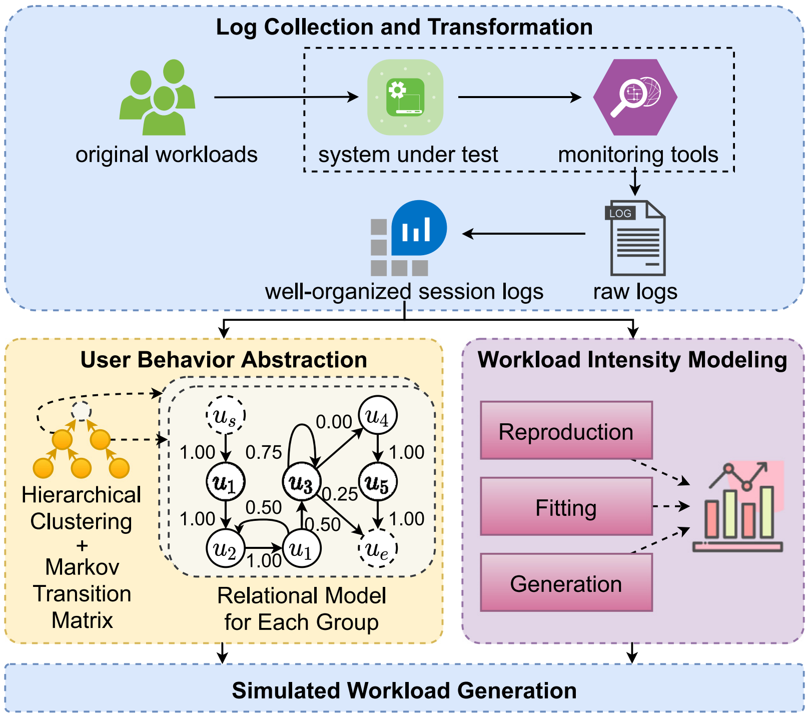
Log Collection and Transformation
original workloads
system under test
monitoring tools
well-organized session logs
raw logs
User Behavior Abstraction
Hierarchical Clustering + Markov Transition Matrix
Relational Model for Each Group
Workload Intensity Modeling
Reproduction
Fitting
Generation
Simulated Workload Generation

Fig. 2. The architecture of the LWS framework.

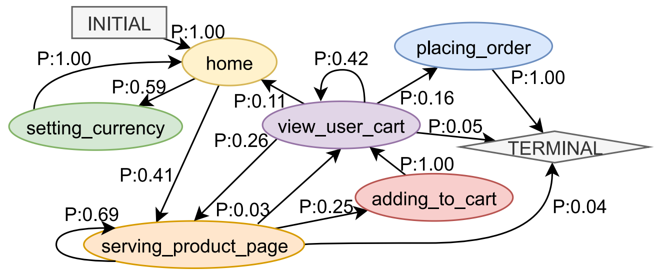

Fig. 3. The Markov probabilistic transition graph constructed on the dataset $\mathcal{A}$ in the case study.

4.2. User behavior abstraction

Suppose there are N_u types of user behaviors for $\mathcal{T}$. Inspired by Markov Chains, the simplest way to abstract user behaviors is to construct a $(N_u + 2) \times (N_u + 2)$ probabilistic transition matrix denoted by $\boldsymbol{A}$. The extra two columns/rows represent the dummy nodes of "start" (denoted by u_s) and "end" (denoted by u_e) for the start and end of a user behavior sequence, similar to the initial Markov state and the exit Markov state. Each row $\boldsymbol{A}_{r,\_}$ or each column $\boldsymbol{A}_{\_,c}$ corresponds to a certain type of user behavior, and each element $A_{r,c} \in \boldsymbol{A}$ is the transition probability from the user behavior u_r to u_c. Since there will be no node preceding u_s, the transition probability from any node to u_s must be 0. Similarly, since there will be no node following u_e, the transition probability from u_e to any node must be 0. The extraction of S starts from the node of u_s and ends as long as the node of u_e is selected. Refer to Fig. 3 for an example.

However, there are two main drawbacks in the above vanilla abstraction method as follows:

- **The Impact of Different Groups of Users:** Real-world users typically have different preferences which can be divided into different groups. For example, some users just browse without purchasing, while others purchase their essential items. The vanilla abstraction method ignores differences in behaviors and proportions of different user groups.
- **The Neglect of Possible Temporal Invariants:** For example, an item has to be added to the cart (denoted by $u_{add\_to\_cart}$) before the customer places the order (denoted by $u_{placing\_order}$). However, in Fig. 3, the behavior sequence $[u_s, u_{home}, u_{serving\_product\_page}, u_{view\_user\_cart}, u_{placing\_order}, u_e]$ is possible which violates the above restriction. The reason for this is that no temporal invariant has been taken into consideration when transiting between nodes.

To address these problems, we introduce a user behavior abstraction method, grouping users by Hierarchical clustering based on the Markov transition matrix and establishing a relational model for each user group containing pre-defined temporal invariants as follows.

4.2.1. User grouping

To identify different groups of users, each user behavior sequence needs to be represented as feature embedding for (dis) similarity or "distance" computation. Inspired by the behavior model in WESSBAS, we calculate the $(N_u + 2) \times (N_u + 2)$ Markov probabilistic transition matrix $\dot{\boldsymbol{A}}$ for each user behavior sequence and flatten $\dot{\boldsymbol{A}}$ to a vector $\dot{\boldsymbol{v}}$ by Eq. (1) as feature embedding where $\dot{A}_{r,c}$ is the element of $\dot{\boldsymbol{A}}$ in the rth row and the cth column and $\dot{v}_i$ is the ith element of $\dot{\boldsymbol{v}}$.

$$\dot{A}_{r,c} = \dot{v}_{r\times(N_u+2)+c} \tag{1}$$

Based on the above feature embedding, we can compute the user behavior sequence similarity and identify different user groups. Due to the natural hierarchy of user behaviors (Kang et al., 2010), websites (Lee et al., 2011) and user profiles (Gu et al., 2020), we build on a typical hierarchical clustering algorithm, agglomerative clustering which adopts the bottom-up strategy to organize data into a tree structure (Xu and Wunsch, 2005). All N_s user behavior sequences are divided into N_s clusters at first. Then the cluster pair (C_i, C_j) with the minimal variance calculated by Eq. (2) is found where $\dot{N}$ denotes the number of clusters, C_i denotes the ith cluster, $\dot{\boldsymbol{v}}_h$ denotes the feature embedding of the hth user behavior sequence in the cluster, $\boldsymbol{m}_{C_p}$ denotes the central vector of the cluster C_p and $\|\cdot\|$ denotes the two-norm of a vector.

$$\Delta(C_i, C_j) = \min_{1\le p,q\le \dot{N}} \Big(\sum_{h\in C_p\cup C_q} \left\| \dot{\boldsymbol{v}}_h - \boldsymbol{m}_{C_p\cup C_q} \right\|^2 - \sum_{h\in C_p} \left\| \dot{\boldsymbol{v}}_h - \boldsymbol{m}_{C_p} \right\|^2 - \sum_{h\in C_q} \left\| \dot{\boldsymbol{v}}_h - \boldsymbol{m}_{C_q} \right\|^2 \Big) \tag{2}$$

Then C_i and C_j are merged into a new cluster and the new cluster pair between the new cluster and the other clusters is searched for a new merger. The process is repeated until all user behavior sequences are in N_c clusters where N_c is the expected number of groups.

4.2.2. Relational model establishing for each user group

For each group of user behavior sequences identified in Section 4.2.1, we introduce Synoptic (Schneider et al., 2010) which generates a relational model to model user behaviors with temporal invariants. Three kinds of invariants are pre-defined and mined in user behavior sequences:

- **a Always Followed by b:** Whenever the behavior type a appears, the behavior type b always appears later in the same user behavior sequence.
- **a Never Followed by b:** Whenever the behavior type a appears, the behavior type b never appears later in the same user behavior sequence.
- **a Always Precedes b:** Whenever the behavior type b appears, the behavior type a always appears before b in the same user behavior sequence.

To mine the above invariants, each user behavior sequence is traversed once to collect the following counts:

- $\forall a$, OC[a] denoting the number of user behavior instances of a.
- $\forall a, b$, FO[a][b] denoting the number of user behavior instances of a which are followed by one or more user behavior instances of b.
- $\forall a, b$, PR[a][b] denoting the number of user behavior instances of n which are preceded by one or more user behavior instances of a.

Then the invariants are mined by Eq. (3).

$$\begin{aligned} a\ \textbf{Always Followed by}\ b &\Leftrightarrow \mathrm{FO}[a][b] = \mathrm{OC}[a] \\ a\ \textbf{Never Followed by}\ b &\Leftrightarrow \mathrm{FO}[a][b] = 0 \\ a\ \textbf{Always Precedes}\ b &\Leftrightarrow \mathrm{PR}[a][b] = \mathrm{OC}[b] \end{aligned} \tag{3}$$

After mining the invariants, the probabilistic transition matrix is also constructed as the adjacency matrix of the initial graph $\mathcal{G}(\mathcal{V}, \mathcal{E})$ where $\mathcal{V}$ denotes the vertex set and $\mathcal{E}$ denotes the edge set. Refinement and coarsening operations are performed in eliminating transition processes that violate the invariants (i.e. counterexamples) based on the initial graph as shown in Fig. 4. In the refinement process (lines 1–16), the Bisim algorithm (Schneider et al., 2010) is applied to eliminate counterexamples by generating new partition graphs. A partition is the splitting of the vertex in $\mathcal{V}$, belonging to the same user behavior type but corresponding to different instances. First *findCounterexample*() attempts to find at least one counterexample for each invariant by traversing the vertices based on Breadth-First Search (BFS). For each counterexample, *findSplit*() attempts to find a valid split that can eliminate the counterexample. The longest prefix of counterexample that does not violate any invariant is identified and the last vertex

```
**Input:** initial graph $\mathcal{G}(\mathcal{V},\mathcal{E})$; invariant set $\mathcal{I}$
**Output:** graph $\mathcal{G}(\mathcal{V},\mathcal{E})$ satisfying all invariants in $\mathcal{I}$
    /* Step 1: Refinement */
 1: set $\mathcal{CE} = findCounterexample(\mathcal{G}(\mathcal{V},\mathcal{E}),\mathcal{I})$
 2: **while** $\mathcal{CE}$ is not $\emptyset$ **do**
 3:     list $sp$ = []
 4:     **for** $ce$ in $\mathcal{CE}$ **do**
 5:         $sp$.append($findSplit(\mathcal{G}(\mathcal{V},\mathcal{E}), ce)$)
 6:     **end for**
 7:     **if** no valid split in $sp$ **then**
 8:         select a split $s$ arbitrarily
 9:         $\mathcal{G}(\mathcal{V},\mathcal{E}) := split(\mathcal{G}(\mathcal{V},\mathcal{E}), s)$
10:     **else**
11:         **for** $s$ in **sp do**
12:             $\mathcal{G}(\mathcal{V},\mathcal{E}) := split(\mathcal{G}(\mathcal{V},\mathcal{E}), s)$
13:         **end for**
14:     **end if**
15:     $\mathcal{CE} := findCounterexample(\mathcal{G}(\mathcal{V},\mathcal{E}),\mathcal{I})$
16: **end while**
    /* Step 2: Coarsening */
17: bool $cm$ = True
18: **while** $cm$ **do**
19:     **for** $p, q$ in distinct vertex combinations of $\mathcal{V}$ **do**
20:         **if** $p \neq q$ and $p, q$ belong to the same type **then**
21:             $\mathcal{G}'(\mathcal{V}',\mathcal{E}') = merge(\mathcal{G}(\mathcal{V},\mathcal{E}), p, q)$
22:             set $\mathcal{CE}' = findCounterexample(\mathcal{G}'(\mathcal{V}',\mathcal{E}'),\mathcal{I})$
23:             **if** $\mathcal{CE}'$ is not $\emptyset$ **then**
24:                 $cm$ := False
25:             **else**
26:                 $\mathcal{G}(\mathcal{V},\mathcal{E}) := \mathcal{G}'(\mathcal{V}',\mathcal{E}')$
27:                 $cm$ := True
28:                 **break**
29:             **end if**
30:         **end if**
31:     **end for**
32: **end while**
33: **return** $\mathcal{G}(\mathcal{V},\mathcal{E})$
```

Fig. 4. The refinement and coarsening algorithm.

of the prefix is selected to be the candidate split. Then the new partition graph is generated based on the split. If there is no valid split but still exists counterexamples, the new partition graph is generated based on an arbitrary split. The above process is repeated until there exists no counterexample in the partition graph.

In the coarsening process (lines 17–32), the kTails algorithm (Biermann and Feldman, 1972) is applied to reduce the number of partitions for the sake of brevity. Each pair of two different partitions belonging to the same user behavior type is chosen to merge. If there exist new counterexamples in the merged graph, the merge operation is rolled back. Finally, the most concise graph with no invariant violations is generated which is the abstraction of user behaviors.

Synoptic is not the only choice for abstraction. To meet the actual requirements of the SUT, more (or fewer) temporal invariants can be applied to improve the robustness of the generated relational model. For example, Perfume (Ohmann et al., 2014) proposes invariants with constrained resource measurements as well as WESSBAS proposes the invariant learning guards and actions (GaAs) which needs more business knowledge. However, it is impossible to find the exactly right and sufficient invariants because each invariant is designed for special business scenarios specific to the SUT. Expert knowledge of the SUT has a positive effect on the choice of invariants.

4.3. Workload intensity modeling

For better intensity modeling, we propose three methods to model the workload intensity I from different perspectives, namely *Reproduction*, *Fitting* and *Generation*.

4.3.1. Reproduction

In the reproduction method, we want to reproduce the time series of the original intensity I exactly for workload simulation. In other words, the simulated intensity can be seen as the translation of the original intensity along the x-axis to a new time interval. The goal seems to be clear and straightforward, but it is almost impossible to achieve in reality because of the difference in session lengths (the number of user behaviors belonging to a session) or thinking times between the original workload and the simulated workload. For example, after an interval of 30 min, the original intensity may ramp down to 0 active sessions, but we cannot make sure that the sessions of simulated workload are also finished.

To simplify the problem, we follow the principle of Occam's Razor and only consider the start time of each session rather than the duration. That is, $I(t)$ denotes the number of sessions which starts in the time of t rather than the number of active sessions in the reproduction method (as well as the other two methods). Suppose that the interval between the start time of the ith session and the $(i+1)$th session is $\triangle t$ in the original intensity. In the simulated intensity generated by the reproduction method, the interval between the start time of S_i and S_{i+1} is also expected to be $\triangle t$.

To make sure that the domain of I, denoted by $t \in [t_s, t_e]$, can be divided into successive equally spaced points to be a standard time series, we set up an array of initially empty buckets. Each of them represents a time span of δ seconds, so from left to right each bucket covers the range of $[t_s, t_s+\delta)$, $[t_s+\delta, t_s+2\times\delta)$, $\cdots$, $[t_e-\delta', t_e]$ where $\delta' = (t_e - t_s)\ mod\ \delta$ (*mod* means the modulo operation). Then we go over the start time of each session and put each session in its bucket. In this way, $I(t)$ discards the fine-grained information on the start time of each session, but it can describe the overall intensity in the form of a standard time series.

If the original workload consists of N_S sessions, we also have to extract N_S user behavior sequences from the relational model to make sure that the total number of sessions is consistent. Consequently, we can reproduce the original intensity with respect to the session start time.

4.3.2. Fitting

Sometimes we are not only interested in reproducing the original intensity, but also interested in the performance of the SUT if we deliberately change the original intensity. For example, we may want to produce a workload that is longer than the original workload and increase the concurrent user capacity to see how the memory usage will change under the new workload. The new workload relies on the characteristics of the original workload rather than the simple translation. To achieve this goal, we propose the fitting method to learn the characteristics of the original intensity based on basic mathematical expressions. The first step is to decompose the original intensity into three distinct components including seasonality, trend, and noise based on time series decomposition algorithms such as RobustSTL (Wen et al., 2019). This step is to make sure that we can take a deeper investigation into the characteristics of the original intensity. For example, the intensity in an online game may have a significant repeating short-term cycle on weekends, and we can analyze the seasonality independently to increase the peak on weekends but keep the online players on weekdays unchanged. The next step is to use a set of basic mathematical expressions such as polynomials to fit the targeted time series and choose the most suitable expression. Quasi-Newton methods (Dennis and Moré, 1977) are introduced to resolve the non-linear equations so that we can resolve the time series to a parameterized mathematical expression. At last, we can adjust the expression parameters to control the shape of the targeted time series freely.

For the convenience of user interaction when fitting the time series, we develop a tool with a visual interface of windows, as shown in Fig. 5. The intensity can be imported from a data file and subsequently decomposed into different components. It is worth mentioning that the decomposition algorithm usually requires the parameter of "period" as the prior knowledge of the time series. To compute the period value, we perform the fast Fourier transformation and the largest peak in the frequency domain can indicate the possible period. Then, a decent interval rather than the whole range of the time series should be specified before fitting. The reasons are twofold: (1) The shape of a time series may be too complex for a basic mathematical expression to fit. It is better to divide the time series into multiple non-overlapped intervals and fit them one by one. (2) The shorter the interval is, the simpler the expression is. Sometimes we are more interested in the shape of a specific interval, and a simple expression without higher terms is easier to understand. In the top middle panel, a total number of 25 fitting expressions are provided. The tool can choose the best one automatically based on the metric of RMSE. In the middle panel, the parameters are displayed to be adjusted. The right panel displays the fitting results as text, and the bottom panel visualizes the fitting results.

Unlike the reproduction method, even if the original workload consists of N_S sessions, the number of S extracted from the relational model is not necessarily N_S in the fitting method because the shape of the original intensity has been changed by the decomposition algorithm.

4.3.3. Generation

In the generation method, we create the new intensity from scratch based on self-specified characteristics. In this way, we can customize the shape of the simulated workload. For different known parameters and required characteristics of the new intensity, two existing methods of time series generation, LIMBO (Kistowski et al., 2017) and TSAGen (Wang et al., 2021), can be integrated into the generation method as follows.

(1) LIMBO-based Method: We follow LIMBO which allows a DSL-based workload intensity definition and make some changes for better intervention. The workload intensity is represented with the trend component *trend*, the season component *season*, the burst component *burst*, and the noise component *noise*. The additive combinator is applied to merge above components:

$$I(t) = trend(t) + season(t) + burst(t) + noise(t) \tag{4}$$

Table 1 shows the details of each component with related parameters and the generation process where *mod* means the modulo operation. The noise component is generated by sampling from the Gaussian distribution $N(\frac{\eta_9+\eta_8}{2}, \frac{\eta_9-\eta_8}{6})$ where 99.7% of data occurs within three standard deviations of the mean constrained by the minimum value η_8 and the maximum value η_9. The other three components are generated by interpolation functions such as polynomials. The length of the trend component is in multiples of seasonal iterations which is calculated by $\eta_1 \times \eta_2$. Since the determination of nonlinear interpolation functions generally requires three points, three representative points, the starting point, the endpoint, and the midpoint whose values are c_1, c_2, and c_3 respectively are selected for the interpolation of *trend*. The generation of the seasonal component is shown in Fig. 6.

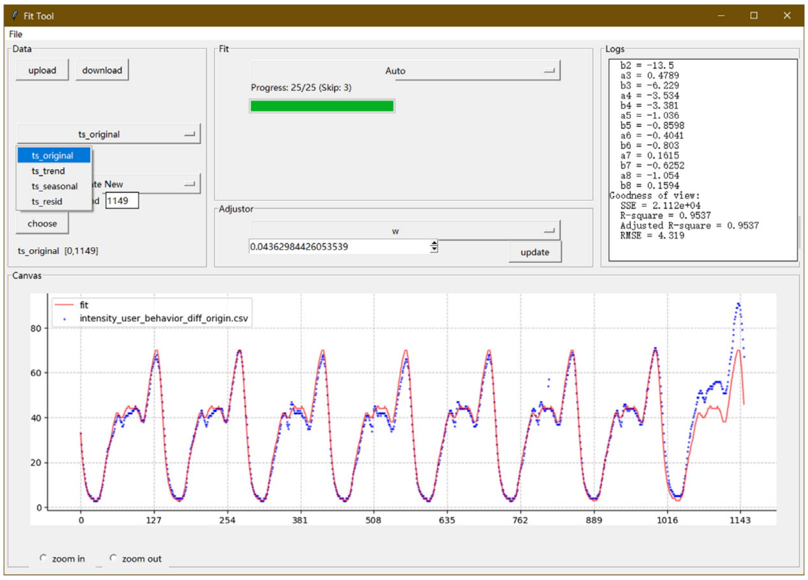

```
  b2 = -13.5
  a3 = 0.4789
  b3 = -6.229
  a4 = -3.534
  b4 = -3.381
  a5 = -1.036
  b5 = -0.8598
  a6 = -0.4041
  b6 = -0.803
  a7 = 0.1615
  b7 = -0.6252
  a8 = -1.054
  b8 = 0.1594
Goodness of view:
  SSE = 2.112e+04
  R-square = 0.9537
  Adjusted R-square = 0.9537
  RMSE = 4.319
```

Fig. 5. The developed tool for the fitting method.

Table 1
Details of the generation method based on LIMBO.

Component	Parameter	Description	Generation
trend	η_1 η_2 c_1 c_2 c_3 g_1	number of seasonal periods in one trend seasonal period (same as that in *season*) starting point value endpoint value midpoint value interpolation function for trend shape	$trend(t) = g_1(t - t_s, \eta_1 \times \eta_2, c_1, c_2, c_3)$
season	η_2 η_3 η_4 c_4 c_5 c_6 c_7 g_2	period number of peaks interval between first and last peaks starting and end value of one iteration trough between two peaks first peak last peak interpolation function for seasonal shape	$season(t) = \begin{cases} g_2(t_c, \eta_s, c_4, c_5, c_6), 0 \le t_c < \eta_s \\ g_2(t_c, \eta_r, c_5, c_5, c_6 + \frac{(i+1)(c_7-c_6)}{\eta_3 - 1}), \\ \quad i \times \eta_r \le t_c - \eta_s < (i+1) \times \eta_r \\ g_2(t_c, \eta_s, c_5, c_4, c_7), \eta_2 - \eta_s \le t_c \le \eta_2 \end{cases}$ where $t_c = (t - t_s) \bmod \eta_2$, $\eta_s = 0.5 \times (\eta_m + \eta_r)$, $\eta_m = \eta_2 - \eta_4$, $\eta_r = \eta_4/(\eta_3 - 1)$ and $i < \eta_3 - 2$, $i \in \mathbb{N}$
burst	η_5 η_6 η_7 c_8 g_3	first burst peak offset interval between two bursts burst width burst peak interpolation function for burst shape	$burst(t) = \begin{cases} g_3(t_c, \eta_7, 0, 0, c_8), 0 \le t_c \le \eta_7 \\ 0, t_c > \eta_7 \end{cases}$ where $t_c = (t - t_s - \eta_5 + 0.5 \times \eta_7) \bmod \eta_6$
noise	η_8 η_9	minimum value maximum value	$noise(t) = Normal(\frac{\eta_9+\eta_8}{2}, \frac{\eta_9-\eta_8}{6})$

Given the first peak c_6, the lask peak c_7, and the number of peaks η_3, additional peaks are derived from linear interpolation which is the most intuitive. The distance between the starting and the first peak is assumed to be equal to that between the last peak and the end, denoted by $0.5 \times \eta_m$. In the boundary interval between the starting and the first trough (or the last trough and the end), *season* is generated by interpolation of the boundary point, the peak, and the trough. In the intervals between two adjacent troughs, *season* is generated by interpolation of the peak and troughs. The burst component defines recurring bursts under the assumptions of the same recurring interval η_6 and the axisymmetric burst. Only the point in the burst has the non-zero value which is also generated by the interpolation function given the burst width η_7 and the burst peak c_8 (the starting and the end value of a burst is 0). Besides, the first burst peak offset η_5 controls the offset and is under the assumption of $\eta_5 < \eta_6$.

(2) TSAGen-based Method: TSAGen is a time series generation tool for controllable and anomalous key performance indicator data generation. For the property in the task of workload simulation, only the normal data generation stage is integrated into workload intensity modeling. To be specific, the workload intensity is represented with the trend component *trend*, the seasonal component *season*, and the noise component *noise* of the same length:

$$I(t) = trend(t) + season(t) + noise(t) \tag{5}$$

Details of each component with related parameters and the generation process are shown in Table 2. The trend component is generated by a linear function by setting the level and the scope. The seasonal component is generated by connecting cycles whose shape is modeled by the Random Midpoint Displacement Fractal (RMDF) algorithm (Fournier et al., 1982). $\sum \bigoplus$ means multiple cycles are concatenated in order. a_i and f_i are the drift factors of amplitude and frequency sampled from the uniform distributions $U(1, 1 + k_1)$ and $U(1, 1 + k_2)$ respectively for representing drifts such as holiday effects. $cycle_{i,f_i*1/\theta_4}$ denotes the ith cycle of the length $f_i * 1/\theta_4$ generated by sampling (marked as $sample_i$) on the function F_{RMDF} obtained from the RMDF algorithm. Fig. 7 displays the RMDF process. Given two initial points $P_1(0, 0)$, $P_2(1, 0)$, the control point in the perpendicular bisector

Table 2
Details of the generation method based on TSAGen.

Component	Parameter	Description	Generation
trend	θ_1 θ_2	level of trend slope of trend	$trend(t) = \theta_1 + \theta_2 \times (t - t_s)$
season	θ_3 θ_4 θ_5 k_1 k_2 d_1 d_2	amplitude frequency number of cycle drift degree of amplitude drift degree of frequency recursion depth forking depth	$season(t) = (\sum_{i=1}^{\theta_5} \bigoplus(\theta_3 \times a_i)cycle_{i,f_i*1/\theta_4})_{t-t_s}$, where $a_i \sim U(1, 1+k_1), k_1 \in [0, +\infty)$, $f_i \sim U(1, 1+k_2), k_2 \in [0, +\infty)$, and $cycle_{i,j} = sample_i(F_{RMDF}(d_1, d_2), j)$
noise	θ_6 θ_7 θ_8	skewness location scale	$noise(t) = Gamma(\theta_6, \theta_7, \theta_8)$

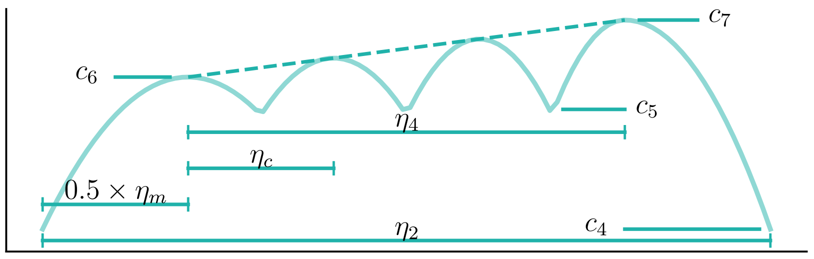

Fig. 6. Seasonal component of the LIMBO generation method.

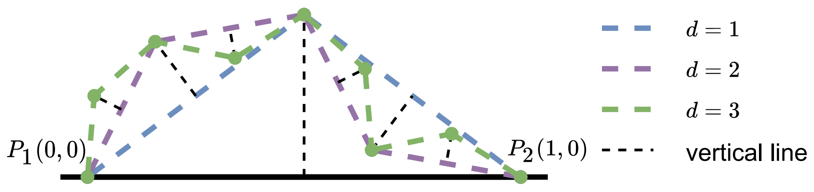

Fig. 7. The RMDF process. The black dotted line represents the perpendicular bisector. Blue, purple and green lines represent curves generated by setting $d = 1, 2, 3$ in RMDF respectively. (For interpretation of the references to color in this figure legend, the reader is referred to the web version of this article.)

is chosen. For a relatively smooth shape, the distance between the control point and the midpoint is sampled from the Gaussian distribution $N(0, 0.25)$ and decreases by half each recursion. Through trigonometric functions and coordinate operations, the function of the curve which connects the initial points and the control point is generated (refer to the blue lines in Fig. 7 for an example). In each new interval generated by adjacent initial points and control points, the process is repeated recursively which is controlled by the recursion depth d (refer to the purple and yellow lines in Fig. 7 for an example). For small differences in shape modeling, a base function sharing by all cycles is generated by setting the certain recursion depth d_1. Then d_2 recursions are applied in the base function for each cycle. Based on parameters $\theta_3, \theta_4, \theta_5, k_1, k_2$ controlling characteristics and d_1, d_2 controlling shapes, the seasonal component is generated where the value at the timestamp t is the $(t - t_s)$th element. The Pearson type III distribution, also known as the Gamma distribution, is used to generate the noise component due to the nonnegativity of Gamma-distributed random variables and the controllable statistical properties of the Gamma distribution. Given the skewness θ_6, the location θ_7, and the scale θ_8, the probability density function can be calculated. Then the noise component is generated based on the probability density function.

Similar to the fitting method, the number of S extracted from the relational model depends on the generated intensity rather than the original intensity.

4.3.4. Think time

Not only is the time attribute of a session characterized by the start time, but also by think times between consecutive user behaviors. The aforementioned three methods have modeled the workload intensity in terms of the session start time. Transitions between consecutive user behaviors within a session should also be annotated with the think time. For N_u types of user behaviors, think times in each session can be denoted by a $N_u \times N_u$ matrix $\boldsymbol{T}$ where the element $T_{r,c}$ in the rth row and the cth column denotes the think time from the user behavior u_r to the user behavior u_c. To simplify the problem, we assume think times of different user behavior pairs share the same distribution and all think times can be denoted as a random variable τ. To model the distribution of think times, we use the non-parametric kernel density estimator (KDE) $\widehat{f}_h(\tau)$:

$$\widehat{f}_h(\tau) = \frac{1}{n_{tt}} \sum_{i=1}^{n_{tt}} \phi_h\left(t - t_i\right) = \frac{1}{n_{tt} h} \sum_{i=1}^{n_{tt}} \phi\left(\frac{t - t_i}{h}\right) \tag{6}$$

where n_{tt} is the number of think times (or the number of two consecutive requests) in the original workload, h is the bandwidth and ϕ is the kernel. We define ϕ as the standard normal density $\phi(\tau) \sim N(0, 1)$:

$$\phi\left(\tau\right) = \frac{1}{\sqrt{2\pi}} e^{-\frac{1}{2}t^2} \tag{7}$$

To find the ideal bandwidth h, the rule-of-thumb approach (Silverman, 1998) is applied by estimating standard deviation σ_{tt} from the think time in the original workload:

$$h = 1.06 \sigma_{tt} {n_{tt}}^{-1/5} \tag{8}$$

4.4. Simulated workload generation

With the preliminaries of user behavior abstraction and workload intensity modeling, we can generate the simulated workload. Given user groups $\{C_1, C_2, \cdots, C_{N_c}\}$ identified in Section 4.2.1 and the corresponding numbers of user behavior sequences $\{\hat{N}_1, \hat{N}_2, \cdots, \hat{N}_{N_c}\}$, the probability of each simulated user behavior sequence belonging to the C_i cluster is $\hat{N}_i / \sum_{j=1}^{N_c} \hat{N}_j$. After determining the user group, we can extract the user behavior sequence S from the relational model of the group using the idea of Depth-First Search (DFS). We start traversal from the dummy node u_s and look for its adjacent nodes. According to the transition probability, we move to the next node and continue this loop until the dummy node u_e is selected. We do not mark any node as visited in the search, so it is possible that a node may be visited repeatedly when there exists a cycle. This strategy guarantees the diversity of generated user behavior sequences. For each S, we need to perform a DFS, and the value of $I(t)$ decides how many S we need to extract for the bucket containing the timestamp of t.

For the ith bucket which represents the time span of $[t_s + (i-1) \times \delta, t_s + i \times \delta)$, assume there are k_i sessions that belong to this bucket in the simulated workload. If all k_i sessions start at the timestamp of $t_s + (i-1) \times \delta$, the user concurrency will be skewed to the left point of each interval especially when δ is set to a large value or $I(t_s + (i-1) \times \delta)$ is too large. To ensure the stability of $\mathcal{T}$, we suggest distributing each session evenly in the bucket. Let $\triangle t_i = \delta / k_i$. Then, in the ith bucket, the first session starts at $t_s + (i-1) \times \delta$, the second session starts at $t_s + (i-1) \times \delta + \triangle t_i$ and so on. The duration of each session is not constant because of the diversity of S and the probabilistic think time, but we do not need to pay attention to when a session ends. We also design a domain-specific language (DSL) to describe the workload features in a human-readable way. Non-experts just need to submit a file following the grammar rules for quick execution of LWS. For more details, please refer to Supplemental materials.

5. Case study

In this section, we apply the proposed framework LWS to a session-based application and aim to address the following research questions:

- **RQ1:** How accurately does the simulated workload generated by LWS match the original workload?
- **RQ2:** How effective is the intervention of the simulated workload generated by LWS?
- **RQ3:** How do different workload intensity modeling methods impact the effectiveness of the intervention?

5.1. Experiment setup

5.1.1. Benchmark system

Our studies are conducted in an open-source cloud-native microservices demo application, Hipstershop (also known as Online Boutique).[6] It is a typical web-based e-commerce application widely used in research on the microservice operation. It consists of 10 microservices written in Java, Python, Go, Node.js, and C#, and provides an extra microservice for original workload generation. For each user session, a unique session ID will be generated automatically and recorded in logs. We deploy Hipstershop in an open-source cloud-native system Kubernetes[7] with 5 physical machines and 4 virtual machines. Monitoring tools including Elasticsearch, Filebeat, Prometheus[8] and Jaeger[9] are also deployed in the Kubernetes for monitoring data collection. We implement LWS with Python and deploy the application on another physical server. The details of the deployment environment are shown in Table 3. We have also summarized the detailed resource recommendations and requirements, as well as the related deployment processes and files. For more details, please refer to Supplemental materials.

Table 3
Details of the deployment environment.

System	Component	Detail
Kubernetes	1 physical master	64-core 2.30 GHz CPU, 64 GB RAM
	4 physical nodes	4-core 2.66 GHz CPU, 8 GB RAM
	4 virtual nodes	4-core 2.10 GHz CPU, 16 GB RAM
	Hipstershop	4 pod replicas for each microservice
	Elasticsearch	version 7.13.2
	Filebeat	version 7.13.2
	Prometheus	version 2.10.0
	Jaeger	version 1.28
LWS Driver	1 physical server	64-core 2.40 GHz CPU, 64 GB RAM
	Python	version 3.6.9

5.1.2. Dataset

We use two datasets $\mathcal{A}$ and $\mathcal{B}$ as subjects where $\mathcal{A}$ is the well-designed original workload and $\mathcal{B}$ is the real-world workload in the production system:

(1) Dataset $\mathcal{A}$: We use K6,[10] an open-source load testing tool, to simulate a real-world load on Hipstershop as the original workload. The original user behavior sequence S consists of 7 to 20 user behaviors along with 0 to 11 automatic redirections, and the think time τ is generated independently and identically from $\phi(\tau) \sim N(5, 2)$. To avoid the negative and exceptional value, the think time will be resampled from $\phi(\tau) \sim N(5, 2)$ until it falls within the interval [1, 15]. Both the K6 script running for 3 h and 40 min in total and the scenario with excellent statistical properties such as multiple peaks, obvious seasonality and trend changes which are intuitive and common in real production workloads (Feng et al., 2022) have been applied in 2022 CCF AIOps Challenge.[11] The number of virtual users ramps up from 0 to 60 in 10 minutes, keeps 60 for 40 min, ramps down from 60 to 20 in 10 min, keeps 20 for 20 min, ramps up from 20 to 80 in 10 min, keeps 80 for 40 min, ramps down from 80 to 20 in 10 min, keeps 20 for 20 min, ramps up from 20 to 60 in 10 min, keeps 60 for 40 min and ramps down from 60 to 0 in 10 min. The user behavior sequence S will not be forcefully interrupted at the boundary of the test duration and the user number changes. In case of skewed metrics and unexpected test results, every $u \in S$ will be executed and K6 will wait for any iterations in progress to finish. Hence, the actual execution time will be little greater than 3 h and 40 min.

(2) Dataset $\mathcal{B}$: The dataset $\mathcal{B}$ is generated based on **UserBehavior**[12] which is a subset of Taobao user behavior data containing millions of user–item interactions during November 25

6 https://github.com/GoogleCloudPlatform/microservices-demo
7 https://kubernetes.io/

8 https://prometheus.io/
9 https://www.jaegertracing.io/
10 https://k6.io/
11 https://www.bizseer.com/index.php?m=content&c=index&a=show&catid=25&id=83
12 https://tianchi.aliyun.com/dataset/dataDetail?dataId=649

to December 03, 2017, offered by Alibaba. Due to the differences in business functions and capacities between the production system of **UserBehavior** and Hipstershop, it is impossible to reproduce the exact workload of **UserBehavior** based on Hipstershop. Therefore, we refer to the workload intensity characteristics of **UserBehavior** as the target of the intervention rather than the complete reproduction. To generate the real-world original workload intensity within the capacity of the benchmark system in Section 5.1.1, we count the number of new concurrent users per 10 min from November 25 to December 03, 2017 (in UTC+8 Zone), multiply each number by 0.02 and round results down for adapting to the load capacity in our benchmark system. We adopt the same strategy in the user behavior and think time in $\mathcal{A}$ and reproduce the workload as the dataset $\mathcal{B}$ as the approximated original workload.

5.1.3. *Evaluation metric*

To evaluate the similarity between the original workload and the simulated workload quantitatively, we introduce two categories of metrics:

(1) Static Metrics: Static metrics are obtained from statistics of generated user behavior sequences and thus they will not be affected by the execution of HTTP requests in the SUT. Two workload characteristics, the session length distribution and the behavior distribution (including the relative invocation frequency of different request types and the number of distinct session types) are applied in static metrics. Regardless of dynamic factors such as the request time consuming, the session length distribution is determined by two important factors: the number of requests per session and think time. For the number of requests per session, we refer to the session metrics used in WESSBAS. The minimum value (denoted by "*Min*"), the maximum value (denoted by "*Max*"), the 25th quartile (denoted by "$Q1$"), the median value (denoted by "$Q2$"), the 75th quartile (denoted by "$Q3$"), the mean value (denoted by "*Mean*") and the 0.95 confidence interval (denoted by "$CI_{0.95}$") are computed for analysis. For the think time, we use the metric Intersection over Union (IoU) which quantifies the degree of overlap between the original think time distribution and the estimated think time distribution for evaluation. For the behavior distribution, we refer to the request count statistics used in WESSBAS. The relative invocation frequency of each request type and the number of distinct session types (denoted by "N_{ds}") are computed. Besides, we record the time cost of user behavior abstraction (denoted by *AbstractionTimeCost*) for the evaluation of efficiency.

(2) Dynamic Metrics: Dynamic metrics are computed by monitoring metrics such as CPU utilization and memory usage in the form of time series collected from the SUT under the workload. Note that the investigation of dynamic metrics in workload simulation is proposed in one of our submitted papers (Li et al., 2023), and thus we directly use its methodology in this work. Monitoring metrics are grouped into two categories by the degree of the correlation with business due to their extreme large quantity and variety (for more details, please refer to Li et al. (2023)) and the linked dataset in Supplemental material section. In each category, the Extend-SBD based on the Shape-based distance (SBD) (Paparrizos and Gravano, 2015) which describes both shape and intensity similarities given the weighting factor α is measured for each metric. Then the weighted average $distance \in [0, 2]$ of the Extend-SBD values in each category is calculated. Lower *distance* shows the higher similarity between workloads. The weighted average calculated from metrics weakly correlated with business is denoted by $ESBD(weak)$, and the weighted average calculated from metrics strongly correlated with business is denoted by $ESBD(strong)$. Given the similarity threshold μ, the normalized similarity score $score \in [0, 1]$ is calculated:

$$score = \frac{\mu}{\mu + distance} \tag{9}$$

For $ESBD(weak)$ and $ESBD(strong)$, the normalized similarity scores are calculated and denoted by $score_w$ and $score_s$ respectively. Higher *score* shows a higher similarity between workloads. The composite score denoted by $score_c$ is calculated by the weighted summation where β is a hyperparameter:

$$score_c = (1 - \beta)score_w + \beta score_s, \beta \in (0, 1] \tag{10}$$

We set $\alpha = 0.5$, $\mu = 1.0$, $\beta = 0.9$ in the following evaluation based on dynamic metrics.

5.2. *RQ1: Accuracy of simulated workload*

The evaluation of simulation accuracy (RQ1) depends on the comparison between the original workload (denoted by OW) in the dataset $\mathcal{A}$ and the simulated workload. The output logs and monitoring metrics under the original workload are collected. Now, we have to assume that we have no idea of the original workload which is specified by the K6 script and try to simulate it via these logs.

5.2.1. *Log collection and transformation*

Using the regex match, we can remove the redundant logs and only keep the HTTP request logs. After that, we group these logs by the field of "session" and sort the logs within each session by the field of "timestamp". Fig. 8 illustrates an example of two consecutive HTTP request logs. We can find some useful patterns: (1) The "http.req.id" field is the unique identifier to group the HTTP requests within a session. (2) Each HTTP group follows a common template where the value of the "message" field is "request started" in the first line and "request complete" in the last line. (3) The "message" field in the middle line indicates a certain type of user behavior, and there are 6 different types of user behaviors in total including "home" "setting currency" "serving product page" "view user cart" "adding to cart" "placing order". Note that "placing order" is always followed by "order placed" in an HTTP group and they refer to the same HTTP request, so we use "placing order" as the name of the user behavior for simplicity. A possible reason for the unnecessary alias in these logs is bad coding practice. At last, a total number of 7013 sessions can be obtained.

5.2.2. *User behavior abstraction*

In addition to the methodology in Section 4.2 (denoted by *SW (HAC/Markov)*, cluster num=3), we perform the following different user behavior abstraction methods for comparison:

- *SW (Monolithic)*: Its user behavior abstraction is based on a monolithic Markov probabilistic transition matrix without clustering and a relational model with Synoptic invariants.
- *SW (HAC/SGT)*: Its user behavior abstraction is based on the Sequence Graph Transform embedding (Ranjan et al., 2022) with the same cluster and relational model construction strategy in Section 4.2 (cluster num=3).
- *WESSBAS*: Its user behavior abstraction is based on the Markov probabilistic transition matrix, the X-means cluster algorithm (the cluster num found is 4), and the relational model with proposed invariants as introduced in Vögele et al. (2018).

```
{"http.req.id": "36ecd0da-f04c-4ba4-a5aa-fbfa2e80f338",
 "http.req.method": "POST", "http.req.path": "/setCurrency", "message":
 "request started", "session": "99c93446-301d-41fd-9f87-39e0cc57823c",
 "severity": "debug", "timestamp": "2022-12-31T09:33:07.135829487Z"}
{"curr.new": "CAD", "curr.old": "USD", "http.req.id": "36ecd0da-f04c-
 4ba4-a5aa-fbfa2e80f338", "http.req.method": "POST", "http.req.path":
 "/setCurrency", "message": "setting currency", "session": "99c93446301d-
 41fd-9f87-39e0cc57823c", "severity": "debug", "timestamp": "2022-12-
 31T09:33:07.136127971Z"}
```

Fig. 8. An example of two consecutive HTTP request logs.

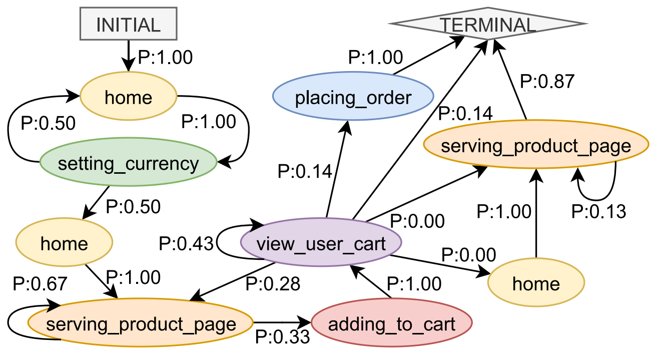

Fig. 9. The relational model of user group 1 in SW (HAC/Markov) constructed on $\mathcal{A}$.

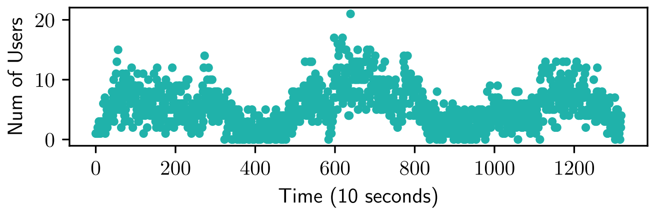

Fig. 10. The intensity via *Reproduction* of $\mathcal{A}$ setting $\delta = 10$.

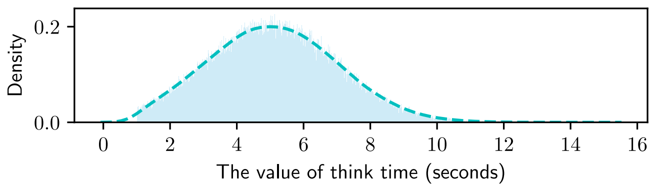

Fig. 11. The modeled probability density function of think times in SW (HAC/Markov) constructed on $\mathcal{A}$.

The resulting user behavior abstraction of user group 1 in *SW (HAC/Markov)* is illustrated in Fig. 9 as an example. $P_{a,b}$ denotes the transition probability from the user behavior u_a to the user behavior u_b. It can be seen from the figure that $P_{a,b}$ equals 0.00 or 1.00 sometimes. If a transition probability has a value less than 0.01, it will be approximated by 0.00. There are two situations that result in a transition probability of 1.00:

- One-to-one Transition: For example, in the original workload, the first user behavior is always "home". Therefore, the transition probability from "initial" to "home" is 1.00.
- Redirection: For example, the reason for the transition probability of 1.00 from "setting_currency" to "home" is that the HTTP request will be redirected to u_b automatically after u_a has been executed. We recommend manually analyzing the frontend code, or sending the HTTP request for u_a to the SUT and then analyzing the output logs or the HTTP status code (such as 302) to identify the redirection operation and avoid redundant user behaviors.

5.2.3. Workload intensity modeling

We use *Reproduction* which contains no intervention when simulating the workload of $\mathcal{A}$. Fig. 10 displays the intensity scatter setting $\delta = 10$. The shape of the workload intensity generated by the reproduction method is intuitively similar to that of the number of virtual users in the original workload. However, the value of the point in the intensity is significantly smaller than the number of virtual users in the original workload. The reason is that the number of users set by K6 describes the concurrency rather than the increment. In other words, K6 will count a user in the concurrency until behaviors belonging to the user finish. Different from K6, each point in the generated intensity describes the increment indicating how many additional users will start their behaviors. Besides, the points in the intensity are intuitively even, which ensures the stability of the simulated workload.

For the think time, we calculate the time difference between the timestamp recorded in the "request complete" log of each behavior and the timestamp recorded in the "request start" log of its next behavior as an approximation. Then we set the bandwidth calculated by Eq. (8) and Fig. 11 displays the estimation result. The dashed line shows the probability density function modeled by KDE and the light blue histogram shows the original distribution of the think time. It can be seen from Fig. 11 that the modeled probability density function can intuitively fit the distribution of the think time well although there exist interval limitations in the original distribution.

5.2.4. Simulated workload generation

We sample 7013 user behavior sequences from the user abstraction model and schedule them by the generated workload intensity. For the simulated workload, the user behavior sequence in each session differs from each other and we need to send each HTTP request in an exact timestamp. Traditional load testing tools which only focus on the number of concurrent users conveniently are not suitable for this task. For example, K6 executes a group of sessions simultaneously from a high level while lacking the fine-grained control of the start time for each HTTP request. As a result, we develop a useful script based on multithread scheduling to execute the simulated workload. The whole process starting from monitoring the application until the simulated workload is acquired is around 9 h, including the original workload (about 3 h and 40 min), collection and transformation of logs and monitoring metrics (about 1 hour with another 20 min waiting for stability in monitoring tools), LWS extraction (about 10 min), and the simulated workload (about 3 h and 40 min). Most of the time cost is in the workload execution and data preparation.

Table 4
Static metrics in terms of the session length distribution and the time cost of user behavior abstraction between the original workload and the simulated workload in $\mathcal{A}$.

Workload Type	*Min*	*Q1*	*Q2*	*Q3*	*Max*	*Mean*	$CI_{0.95}$	*IoU*	*AbstractionTimeCost*
OW	7	9	19	24	31	18.74	[18.56,18.91]	–	–
SW (Monolithic)	4	11	16	24	100	19.29	[19.00,19.58]	73.25%	12.06s
SW (HAC/Markov)	4	9	14	23	155	18.77	[18.41,19.12]	73.46%	26.99s
SW (HAC/SGT)	4	9	15	23	142	18.19	[17.88,18.49]	73.71%	39.27s
WESSBAS	4	10	14	21	93	16.57	[16.33,16.80]	73.45%	24.34s

Table 5
Static metrics in terms of the behavior distribution between the original workload and the simulated workload in $\mathcal{A}$.

Workload Type	adding_to_cart	home	placing_order	serving_product_page	setting_currency	view_user_cart	N_{ds}
OW	9.95%	18.05%	2.98%	39.44%	10.67%	18.92%	131415
SW (Monolithic)	9.82%	17.72%	3.01%	40.03%	10.47%	18.95%	135262
SW (HAC/Markov)	9.81%	18.11%	2.97%	39.85%	10.66%	18.61%	131607
SW (HAC/SGT)	9.78%	18.40%	2.97%	39.60%	10.95%	18.30%	127536
WESSBAS	10.10%	18.72%	2.74%	37.88%	11.89%	18.67%	116179

5.2.5. Quantitative analysis of accuracy

We compare the original workload and the simulated workloads in the dataset $\mathcal{A}$ quantitatively by static metrics and dynamic metrics after simulated workload generation. Static metrics in terms of the session length distribution and the time cost of user behavior abstraction are displayed in Table 4. *SW (HAC/Markov)* performs better than other simulated workloads in *Mean* ($18.74\% \rightarrow 18.77\%, +0.03\%$) and $CI_{0.95}$ ($18.56\% \rightarrow 18.41\%$, -0.15% in the left boundary and $18.91\% \rightarrow 19.12\%$, $+0.21\%$ in the right boundary), and similar to other simulated workloads in *Min*, *Q1*, *Q2*, *Q3*. However, *SW (HAC/Markov)* has a low value of 4 in *Min* and a very high value of 155 in *Max* compared with the original workload. This can be explained by the fact that a few user behavior sequences with low probabilities containing multiple loops can be sampled from the user behavior abstraction as shown in Fig. 9. According to the values in *Q1*, *Q2*, *Q3* and $CI_{0.95}$ of *SW (HAC/Markov)*, the overall differences between session length distributions are not excessive in relation to the extreme values of *Min* and *Max*. Besides, each metric in *WESSBAS* almost has a lower value than that in other simulated workloads. This can be explained by the fact that temporal invariants in *WESSBAS* have stricter limits than Synoptic and longer user behavior sequences are more likely to violate. For the think time of the original distribution and the estimated distribution, the area of intersection is around 73.25% to 73.71% of *IoU*, which means distributions are highly overlapping. Static metrics in terms of the behavior distribution are displayed in Table 5. *SW (HAC/Markov)* has the lowest average difference (0.1267%) among all relative invocation frequencies. Besides, the total number of distinct session types of *SW (HAC/Markov)* has a minimal increase by 0.15% ($131415 \rightarrow 131607$) compared with other workloads. Besides, *WESSBAS* still has a low value of 116179 in N_{ds}, which also shows fewer long sessions are sampled *WESSBAS* due to the stricter limits. For the time cost of user behavior abstraction, *SW (Monolithic)* has the minimal time cost (12.06 s) without clustering and *SW (HAC/Markov)* as well as *WESSBAS* have similar user behavior abstraction time cost (26.99 s and 24.34 s). Compared with the total time of the whole process (around 9 h), the time cost of user behavior abstraction is small and acceptable.

Table 6 shows dynamic metrics between the original workload and the simulated workload in the dataset $\mathcal{A}$. *SW (HAC/Markov)* performs better than other simulated workloads in $ESBD(strong)$ (0.0436), $score_s$ (0.9582), and $score_c$ (0.9431), which also shows *SW (HAC/Markov)* is quite similar with *OW* shows . In metrics weakly correlated with business, *SW (HAC/Markov)* performs worse than other simulated workloads possibly because of the impact on other system processes or applications.

Table 6
Dynamic metrics between the original workload and the simulated workload in $\mathcal{A}$.

Method	$ESBD(weak)$	$score_w$	$ESBD(strong)$	$score_s$	$score_c$
SW (Monolithic)	0.2297	0.8132	0.0481	0.9541	0.9400
SW (HAC/Markov)	0.2376	0.8080	0.0436	0.9582	0.9431
SW (HAC/SGT)	0.2137	0.8239	0.0563	0.9467	0.9345
WESSBAS	0.2300	0.8130	0.1237	0.8899	0.8822

In conclusion, *SW (HAC/Markov)* outperforms other simulated workloads in both static and dynamic metrics, and the similarity between *SW (HAC/Markov)* and *OW* shows the simulated workload generated by LWS can match the original workload accurately.

5.3. RQ2: Effectiveness of intervention

To evaluate the effectiveness of the intervention, we extract the real-world workload intensity characteristics of the dataset $\mathcal{B}$ and use the fitting method and the generation method to provide interventions. Although both the fitting method and the generation method can provide interventions, their different aims lead to different evaluation criteria. The fitting method learns the characteristics of the original intensity. Therefore, both the similarity between the original intensity and the modeled intensity and the similarity between the original workload and the simulated workload need to be measured. Different from the fitting method, the generation method customizes the intensity from the scratch. Therefore, the similarity between the original intensity and the modeled intensity is not important. It is more important that the generation process is simple and the simulated workload is similar to the real-world workload. Therefore, we use simple parameters to generate the workload similar to the real-world original workload for the evaluation of the generation method. For both the fitting method and the generation method, the original workload is approximated by the workload generated by *Reproduction* as described in Section 5.1.2 which is used for comparison. The whole process starting from monitoring the application until the simulated workload is acquired is around 9 h, including the original workload (about 3 h and 20 min), collection and transformation of logs and monitoring metrics (about 1 hour with another 20 min waiting for stability in monitoring tools), LWS extraction (about 40 min), and the simulated workload (about 3 h and 20 min). In the process of LWS extraction, we have invited 10 non-experts with fundamentals of higher mathematics to fit the original intensity and generate intensity intuitively similar to the original intensity. All of them can finish each task in 30 min after reading the 5-minute README file.

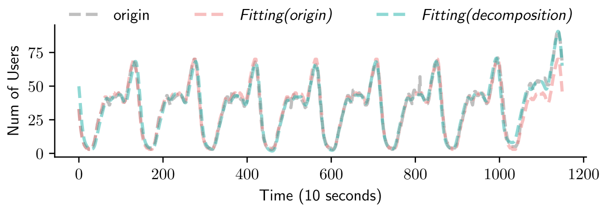

(a) *Fitting* result.

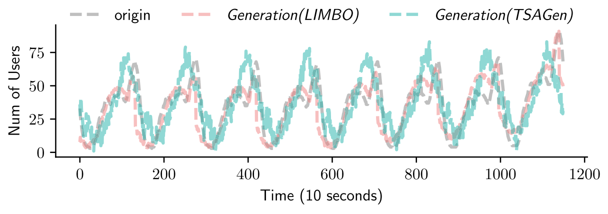

(b) *Generation* result.

Fig. 12. User behavior *Fitting* and *Generation* result.

Table 7
The overall mathematical expressions of fitting the original intensity in the dataset $\mathcal{B}$.

Method	Component	Expression	SSE	R-square	RMSE
Fitting (Origin)	-	Fourier	2.112×10^4	0.9537	4.319
Fitting (Decomposition)	*trend*	Polynomial	79.53	0.9922	0.264
	season	Fourier	296.8	0.9993	0.5121
	noise	Gaussian	1.403×10^4	0.2838	3.498
	merge	$f(x) = trend + season + noise$	1.405×10^4	0.9692	3.541

Table 8
Dynamic metrics between the original workload (approximated by *Reproduction*) and the simulated workload in the dataset $\mathcal{B}$.

Method	$ESBD(weak)$	$score_w$	$ESBD(strong)$	$score_s$	$score_c$
Fitting(Origin)	0.1435	0.8745	0.0123	0.9878	0.9764
Fitting(Decomposition)	0.1113	0.8998	0.0106	0.9894	0.9805
Generation(LIMBO)	0.0989	0.9099	0.0161	0.9840	0.9766
Generation(TSAGen)	0.1400	0.8771	0.0385	0.9629	0.9543

5.3.1. *Fitting*

We use the tool as shown in Fig. 5 to fit the original intensity. To identify the impact of the decomposition step, both fitting the original intensity directly (denoted by *Fitting(Origin)*) and fitting each part decomposed by RobustSTL (denoted by *Fitting(Decomposition)*) are adopted. Table 7 shows the overall mathematical expressions and evaluation metrics including the sum of squares error (denoted by SSE), R-squared value (denoted by R-square), and the root mean square error (denoted by RMSE) of fitting the original intensity. Each mathematical expression is the most suitable one automatically chosen based on RMSE. For detailed expressions, please refer to Supplemental materials. Intensities generated by both *Fitting(Origin)* and *Fitting(Decomposition)* have high R-square (0.9537 and 0.9692), which means that both *Fitting(Origin)* and *Fitting(Decomposition)* can fit the original intensity well. Fig. 12(a) shows the original intensity and fitting results. Intensities generated by both *Fitting(Origin)* and *Fitting(Decomposition)* are similar to the original intensity intuitively. The dynamic metrics between the original workload (approximated by *Reproduction*) and the simulated workload whose intensity is generated by *Fitting* are shown in Table 8. Generally, simulated workloads generated by *Fitting(Origin)* and *Fitting(Decomposition)* have low $ESBD(weak)$ (0.1435 & 0.1113) and $ESBD(strong)$ (0.0123 & 0.0106) as well as high $score_w$ (0.8745 & 0.8998), $score_s$ (0.9878 & 0.9894) and $score_c$ (0.9764 & 0.9805), which shows the similarity between the original workload and the simulated workload.

In conclusion, the original intensity and the modeled intensity by *Fitting* are similar, and the corresponding workloads are similar in dynamic metrics as well, which shows that the intervention by *Fitting* is effective. The detailed differences between *Fitting(Origin)* and *Fitting(Decomposition)* will be discussed in Section 5.4.

5.3.2. *Generation*

Based on the observation of the characteristics of the original intensity (such as the number of cycles is 8 and each cycle length is 144), we choose simple parameters and interpolation functions such as the linear function and the quadratic function to make the generation process simple and generate the workload intensity as similar as possible to the original intensity. For detailed parameters, please refer to Supplemental materials.

It is worth mentioning that the length of the intensity generated by *Generation* is usually different from the original intensity. Therefore, we keep the length of the generated intensity longer than that of the original intensity and select the part whose length is equal to that of the original intensity. Fig. 12(b) shows the original intensity and generation results. The shapes of the original intensity, the intensity generated by LIMBO, and the intensity generated by TSAGen have intuitive overall similarities. However, compared with fitting results as shown in Fig. 12(a), the intensities generated by *Generation* have more deviations from the original intensity. The dynamic metrics between the original workload (approximated by *Reproduction*) and the simulated workload whose intensity is generated by *Generation* are shown in Table 8. Generally, the original workload and simulated workloads generated by *Generation* still have high-level overall similarities (0.9766 & 0.9543 in $score_c$). However, there are certain differences reflected in $ESBD(strong)$ and $score_s$. We will discuss these differences in Section 5.4.

In conclusion, the original workload and the simulated workload whose intensity is generated by *Generation* have high-level overall similarities, which shows that the intervention by *Generation* is effective.

5.4. *RQ3: Impact of intensity modeling methods*

We compare different intensity modeling methods by intensity shapes and dynamic metrics of simulated workloads. As shown in Table 7, the polynomial model and the Fourier series model fit *trend* and *season* in the decomposition pretty well respectively (79.53 and 296.8 in SSE, 0.9922 and 0.9993 in R-square as well as 0.264 and 0.5121 in RMSE). However, the exponential model has poor performance in fitting *noise* in the decomposition (1.403×10^4 in SSE, 0.2838 in R-square as well as 3.498 in RMSE), which is the main source of the deviation in *Fitting(Decomposition)*. *Fitting(Origin)* performs worse than *Fitting(Decomposition)* in SSE, R-square and RMSE. The main reason is the strong seasonality of the Fourier series model for *Fitting(Origin)*. As shown in Fig. 12(a), the original intensity has a noticeable increase near the last peak, which cannot be well modeled within the limitation of the Fourier series model. *Fitting(Decomposition)* can model such intensity well due to the flexibility of decomposition. The dynamic metrics of simulated workloads as shown in Table 8 also reflect the performance differences. The simulated workload with the *Fitting(Origin)* intensity performs worse than that with the *Fitting(Decomposition)* intensity in all dynamic metrics, which also proves that *Fitting(Decomposition)* is more effective than *Fitting(Origin)*.

For the intensity generated by *Generation*, there is a significant increase in deviations as shown in Fig. 12(b). The intensity generated by the TSAGen-based generation method (denoted by *Generation(TSAGen)*) is more irregular, while the intensity generated by the LIMBO-based generation method (denoted by *Generation(LIMBO)*) is smoother. The main reason is that the RMDF process in *Generation(TSAGen)* brings more randomness which is closer to reality and *Generation(LIMBO)* uses interpolation functions with good statistics which are more intuitive and controllable. The simulated workload with the *Generation(TSAGen)* intensity performs worse than that with the *Generation(LIMBO)* intensity in all dynamic metrics as shown in Table 8, which also shows that *Generation(TSAGen)* is more random and uncontrollable compared with *Generation(LIMBO)*.

Although *Fitting* and *Generation* have different aims, both of them can help to generate the simulated workload similar to the original workload. In $ESBD(strong)$, $score_s$ and $score_c$, *Fitting(Decomposition)* still performs better, while *Generation(LIMBO)* even performs better than *Fitting(Origin)*. It is worth mentioning that *Generation* performs better than *Fitting* in $ESBD(weak)$ and $score_w$. The main reason is that there are complex cumulative effects of the simulated workload, other applications, and system events on $ESBD(weak)$ and $score_w$.

In conclusion, *Fitting(Decomposition)* can fit the intensity better than *Fitting(Origin)*, *Generation(LIMBO)* can generate controllable and smooth intensity and *Generation(TSAGen)* can generate irregular intensity with more randomness close to reality. Both *Fitting* and *Generation* can help to generate the effective simulated workload. Besides, we suggest that the original workload should contain typical trends, seasonality, and sudden changes due to their importance in workload intensity modeling. In our practice, the size of logs and metrics in a few hours is at the gigabyte level and suitable to be processed, while more data needs complex tiling and compression technologies. We suggest mapping the original workload into 8 h or less by undersampling.

6. Threats to validity

The threat to internal validity mainly lies in the implementation of LWS. To reduce this threat, we chose integration over rewriting related tools whenever possible, and carefully checked if the same output can be guaranteed with the same input between the original tool and the rewriting component such as TSAGen. Moreover, we carefully checked and tested the code to ensure that the expected output can be obtained for test cases.

The threat to external validity mainly lies in the benchmark system and the user behavior dataset. We chose an open-source cloud-native microservices application widely used in AIOps tasks and used the load testing script that has been applied in an influential AIOps competition as well as a public dataset containing real user behaviors to produce original workloads. We claim we can use LWS for workload simulation in other session-based systems.

The threat to construct validity mainly lies in the evaluation metrics. We chose two categories of metrics from generation and execution perspectives. Due to the large data size, numerous types, and phase shifts in monitoring metrics, we adopted a KPI-based quality evaluation of workload simulation method proposed in one of our submitted paper, giving a comprehensive evaluation result.

7. Conclusion and future work

AIOps plays a critical role in the operation and management of cloud-native systems and microservice-based applications. However, the lack of high-quality datasets with diverse scenarios constrains the development and evaluation of AIOps research. Workload simulation that produces realistic workloads is an important task for continually generating such AIOps datasets. In this paper, we formulate the task of workload simulation and propose a novel framework, LWS, for log-based workload simulation in the session-based system. LWS consists of four components, namely log collection and transformation, user behavior abstraction, workload intensity modeling, and simulated workload generation. Hierarchical clustering based on Markov probabilistic transition matrix is applied to identify user groups and the relational model based on temporal invariants for each group is intended for user behavior abstraction. Three workload intensity modeling methods, namely *Reproduction*, *Fitting*, and *Generation*, are introduced in workload intensity modeling for better intervention. Experiment results on a typical cloud-native microservices application with both the well-designed workload and the real-world workload show that the simulated workload generated by LWS is effective and intervenable.

In our future work, we will investigate the automatic selection of temporal invariants in the relational model in the user behavior abstraction. Moreover, we will explore workload simulation with failures induced by external injection through Chaos engineering or internal orchestration through well-designed business workflows that include faults, which can enrich the failure scenarios and further extend our motivation of generating high-quality AIOps datasets.

CRediT authorship contribution statement

Yongqi Han: Conceptualization, Methodology, Software, Investigation, Data curation, Writing – original draft, Writing – review & editing. **Qingfeng Du:** Methodology, Validation, Resources, Writing – review & editing, Project administration. **Jincheng Xu:** Conceptualization, Methodology, Software, Investigation, Writing – original draft, Writing – review & editing. **Shengjie Zhao:** Validation, Resources, Writing – review & editing. **Zhekang Chen:** Conceptualization, Methodology, Validation, Resources, Data curation, Writing – review & editing. **Li Cao:** Validation, Resources, Data curation, Writing – review & editing. **Kanglin Yin:** Conceptualization, Methodology, Validation, Resources, Data curation, Writing – review & editing. **Dan Pei:** Validation, Resources, Data curation, Writing – review & editing, Project administration, Funding acquisition.

Declaration of competing interest

The authors declare that they have no known competing financial interests or personal relationships that could have appeared to influence the work reported in this paper.

Data availability

We have shared the link to our data in the Figshare. The source code is under the limitations of non-disclosure agreements in the Beijing BizSeer Technology Company

Acknowledgments

This work was supported by National Key R&D Program of China (Grant No. 2020YFB2103300). We also gratefully acknowledge the support of the Beijing BizSeer Technology Company.

Appendix A. Supplemental material

The supplemental materials can be accessed through https://github.com/baiyanquan/LWS. The data of this work can be accessed through https://figshare.com/s/87c50b19706242dc0f1e. The source code of this work is under limitations of non-disclosure agreements in the Beijing BizSeer Technology Company. Please contact us via the email contact@bizseer.com or the telephone number 010-82362970 if needed.

References

Abbors, F., Ahmad, T., Truscan, D., Porres, I., 2012. MBPeT: A model-based performance testing tool. In: VALID 2012-4th International Conference on Advances in System Testing and Validation Lifecycle. pp. 1–8.

Barnert, M., Krcmar, H., 2021. Simulation of in-memory database workload: Markov chains versus relative invocation frequency and equal probability - A trade-off between accuracy and time. In: Proceedings of the ACM/SPEC International Conference on Performance Engineering. pp. 73–80. http://dx.doi.org/10.1145/3427921.3450237.

Biermann, A.W., Feldman, J.A., 1972. On the synthesis of finite-state machines from samples of their behavior. IEEE Trans. Comput. C-21, 592–597. http://dx.doi.org/10.1109/TC.1972.5009015.

Calzarossa, M.C., Massari, L., Tessera, D., 2016. Workload characterization: A survey revisited. ACM Comput. Surv. 48, 1–43. http://dx.doi.org/10.1145/2856127.

Curiel, M., Pont, A., 2018. Workload generators for web-based systems: Characteristics, current status, and challenges. IEEE Commun. Surv. Tutor. 20, 1526–1546. http://dx.doi.org/10.1109/COMST.2018.2798641.

Dennis, Jr., J.E., Moré, J.J., 1977. Quasi-Newton methods, motivation and theory. SIAM Rev. 19, 46–89. http://dx.doi.org/10.1137/1019005.

Draheim, D., Grundy, J., Hosking, J., Lutteroth, C., Weber, G., 2006. Realistic load testing of web applications. In: Conference on Software Maintenance and Reengineering. CSMR'06, pp. 57–67. http://dx.doi.org/10.1109/CSMR.2006.43.

Erradi, A., Iqbal, W., Mahmood, A., Bouguettaya, A., 2019. Web application resource requirements estimation based on the workload latent features. IEEE Trans. Serv. Comput. 14, 1638–1649. http://dx.doi.org/10.1109/TSC.2019.2918776.

Fattah, S.M.M., Bouguettaya, A., Mistry, S., 2020. Long-term IaaS selection using performance discovery. IEEE Trans. Serv. Comput. 15, 2129–2143. http://dx.doi.org/10.1109/TSC.2020.3036677.

Fei, B., Zhu, X., Liu, D., Chen, J., Bao, W., Liu, L., 2020. Elastic resource provisioning using data clustering in cloud service platform. IEEE Trans. Serv. Comput. 15, 1578–1591. http://dx.doi.org/10.1109/TSC.2020.3002755.

Feng, B., Ding, Z., Jiang, C., 2022. FAST: A forecasting model with adaptive sliding window and time locality integration for dynamic cloud workloads. IEEE Trans. Serv. Comput. http://dx.doi.org/10.1109/TSC.2022.3156619.

Fournier, A., Fussell, D., Carpenter, L., 1982. Computer rendering of stochastic models. Commun. ACM 25, 371–384. http://dx.doi.org/10.1145/358523.358553.

Goeva-Popstojanova, K., Singh, A.D., Mazimdar, S., Li, F., 2006. Empirical characterization of session-based workload and reliability for web servers. Empir. Softw. Eng. 11, 71–117. http://dx.doi.org/10.1007/s10664-006-5966-7.

Goldstein, M., Raz, D., Segall, I., 2017. Experience report: Log-based behavioral differencing. In: 2017 IEEE 28th International Symposium on Software Reliability Engineering. ISSRE, pp. 282–293. http://dx.doi.org/10.1109/ISSRE.2017.14.

Gu, Y., Ding, Z., Wang, S., Yin, D., 2020. Hierarchical user profiling for E-commerce recommender systems. In: Proceedings of the 13th International Conference on Web Search and Data Mining. pp. 223–231. http://dx.doi.org/10.1145/3336191.3371827.

Herbst, N.R., Huber, N., Kounev, S., Amrehn, E., 2014. Self-adaptive workload classification and forecasting for proactive resource provisioning. Concurr. Comput.: Pract. Exper. 26, 2053–2078. http://dx.doi.org/10.1002/cpe.3224.

Kang, W., Shin, D., Shin, D., 2010. Detecting and predicting of abnormal behavior using hierarchical Markov model in smart home network. In: 2010 IEEE 17th International Conference on Industrial Engineering and Engineering Management. pp. 410–414. http://dx.doi.org/10.1109/ICIEEM.2010.5646583.

v. Kistowski, J., Herbst, N.R., Kounev, S., 2014. Modeling variations in load intensity over time. In: Proceedings of the Third International Workshop on Large Scale Testing. pp. 1–4. http://dx.doi.org/10.1145/2577036.2577037.

Kistowski, J.V., Herbst, N., Kounev, S., Groenda, H., Stier, C., Lehrig, S., 2017. Modeling and extracting load intensity profiles. ACM Trans. Auton. Adapt. Syst. (TAAS) 11, 1–28. http://dx.doi.org/10.1145/3019596.

Kratzke, N., Quint, P.C., 2017. Understanding cloud-native applications after 10 years of cloud computing - A systematic mapping study. J. Syst. Softw. 126, 1–16. http://dx.doi.org/10.1016/j.jss.2017.01.001.

Lee, C.H., Lo, Y.I., Fu, Y.H., 2011. A novel prediction model based on hierarchical characteristic of web site. Expert Syst. Appl. 38, 3422–3430. http://dx.doi.org/10.1016/j.eswa.2010.08.128.

Li, P., Du, Q., Zhao, S., 2023. KEWS: a method evaluation of workload simulation based on KPIs. http://dx.doi.org/10.48550/ARXIV.2301.06530, https://arxiv.org/abs/2301.06530.

Li, Z., Tian, J., 2003. Testing the suitability of Markov chains as web usage models. In: Proceedings 27th Annual International Computer Software and Applications Conference. COMPAC 2003, pp. 356–361. http://dx.doi.org/10.1109/CMPSAC.2003.1245365.

Li, Z., Zhao, N., Zhang, S., Sun, Y., Chen, P., Wen, X., Ma, M., Pei, D., 2022. Constructing large-scale real-world benchmark datasets for AIOps. http://dx.doi.org/10.48550/arXiv.2208.03938.

Lutteroth, C., Weber, G., 2008. Modeling a realistic workload for performance testing. In: 2008 12th International IEEE Enterprise Distributed Object Computing Conference. pp. 149–158. http://dx.doi.org/10.1109/EDOC.2008.40.

Menascé, D.A., Almeida, V.A.F., Fonseca, R., Mendes, M.A., 1999. A methodology for workload characterization of e-commerce sites. In: Proceedings of the 1st ACM Conference on Electronic Commerce. pp. 119–128. http://dx.doi.org/10.1145/336992.337024.

Notaro, P., Cardoso, J., Gerndt, M., 2021. A survey of AIOps methods for failure management. ACM Trans. Intell. Syst. Technol. 12, 1–45. http://dx.doi.org/10.1145/3483424.

Ohmann, T., Herzberg, M., Fiss, S., Halbert, A., Palyart, M., Beschastnikh, I., Brun, Y., 2014. Behavioral resource-aware model inference. In: Proceedings of the 29th ACM/IEEE International Conference on Automated Software Engineering. pp. 19–30. http://dx.doi.org/10.1145/2642937.2642988.

Paparrizos, J., Gravano, L., 2015. K-shape: Efficient and accurate clustering of time series. In: Proceedings of the 2015 ACM SIGMOD International Conference on Management of Data. pp. 1855–1870. http://dx.doi.org/10.1145/2949741.2949758.

Parrott, C., Carver, D., 2020. Lodestone: A streaming approach to behavior modeling and load testing. In: 2020 3rd International Conference on Data Intelligence and Security. ICDIS, pp. 109–116. http://dx.doi.org/10.1109/ICDIS50059.2020.00021.

Ranjan, C., Ebrahimi, S., Paynabar, K., 2022. Sequence graph transform (SGT): a feature embedding function for sequence data mining. Data Min. Knowl. Discov. 36, 668–708. http://dx.doi.org/10.1007/s10618-021-00813-0.

Reiss, C., Tumanov, A., Ganger, G.R., Katz, R.H., Kozuch, M.A., 2012. Heterogeneity and dynamicity of clouds at scale: Google trace analysis. In: Proceedings of the Third ACM Symposium on Cloud Computing. pp. 1–13. http://dx.doi.org/10.1145/2391229.2391236.

Ruffo, G., Schifanella, R., Sereno, M., Politi, R., 2004. WALTy: a user behavior tailored tool for evaluating web application performance. In: Third IEEE International Symposium on Network Computing and Applications, 2004. (NCA 2004). Proceedings. pp. 77–86. http://dx.doi.org/10.1109/NCA.2004.1347765.

Schneider, S., Beschastnikh, I., Chernyak, S., Ernst, M.D., Brun, Y., 2010. Synoptic: Summarizing system logs with refinement. In: Proceedings of the 2010 Workshop on Managing Systems Via Log Analysis and Machine Learning Techniques. p. 2. http://dx.doi.org/10.1145/1928991.1928995.

Schulz, H., Angerstein, T., Okanović, D., van Hoorn, A., 2019. Microservice-tailored generation of session-based workload models for representative load testing. In: 2019 IEEE 27th International Symposium on Modeling, Analysis, and Simulation of Computer and Telecommunication Systems. MASCOTS, pp. 323–335. http://dx.doi.org/10.1109/MASCOTS.2019.00043.

Schulz, H., Okanović, D., van Hoorn, A., Tůma, P., 2021. Context-tailored workload model generation for continuous representative load testing. In: Proceedings of the ACM/SPEC International Conference on Performance Engineering. pp. 21–32. http://dx.doi.org/10.1145/3427921.3450240.

Shams, M., Krishnamurthy, D., Far, B., 2006. A model-based approach for testing the performance of web applications. In: Proceedings of the 3rd International Workshop on Software Quality Assurance. pp. 54–61. http://dx.doi.org/10.1145/1188895.1188909.

Silverman, B.W., 1998. Density Estimation for Statistics and Data Analysis. Routledge, http://dx.doi.org/10.1201/9781315140919.

Soldani, J., Tamburri, D.A., Van Den Heuvel, W.J., 2018. The pains and gains of microservices: A systematic grey literature review. J. Syst. Softw. 146, 215–232. http://dx.doi.org/10.1016/j.jss.2018.09.082.

Taylor, S.J., Letham, B., 2018. Forecasting at scale. Amer. Statist. 72, 37–45. http://dx.doi.org/10.1080/00031305.2017.1380080.

Vögele, C., van Hoorn, A., Schulz, E., Hasselbring, W., Krcmar, H., 2018. WESSBAS: Extraction of probabilistic workload specifications for load testing and performance prediction—a model-driven approach for session-based application systems. Softw. Syst. Model. 17, 443–477. http://dx.doi.org/10.1007/s10270-016-0566-5.

Wang, C., Wu, K., Zhou, T., Yu, G., Cai, Z., 2021. TSAGen: Synthetic time series generation for KPI anomaly detection. IEEE Trans. Netw. Serv. Manag. 19, 130–145. http://dx.doi.org/10.1109/TNSM.2021.3098784.

Wen, Q., Gao, J., Song, X., Sun, L., Xu, H., Zhu, S., 2019. RobustSTL: A robust seasonal-trend decomposition algorithm for long time series. In: 33rd AAAI Conference on Artificial Intelligence, AAAI 2019, 31st Innovative Applications of Artificial Intelligence Conference, IAAI 2019 and the 9th AAAI Symposium on Educational Advances in Artificial Intelligence. EAAI 2019, pp. 5409–5416. http://dx.doi.org/10.1609/aaai.v33i01.33015409.

Xu, R., Wunsch, D., 2005. Survey of clustering algorithms. IEEE Trans. Neural Netw. 16, 645–678. http://dx.doi.org/10.1109/TNN.2005.845141.

Zhou, J., Zhou, B., Li, S., 2014. LTF: A model-based load testing framework for web applications. In: 2014 14th International Conference on Quality Software. pp. 154–163. http://dx.doi.org/10.1109/QSIC.2014.53.

Yongqi Han is a Ph.D student from Tongji University, Shanghai, China. His main research interests include AIOps, root cause analysis, and knowledge reasoning.

Qingfeng Du is a Professor with the School of Software Engineering, Tongji University, Shanghai, China. His main research interests include AIOps, software testing and big data.

Jincheng Xu is a Ph.D from Tongji University, Shanghai, China. His main research interests include AIOps, text classification and adversarial attacks

Shengjie Zhao is currently a Professor with the School of Software Engineering, Tongji University, Shanghai, China. His research interests include big data, wireless communications, image processing, and signal processing. He is a fellow of the Thousand Talents Program of China.

Zhekang Chen, the leader of Chaos Engineering team from Beijing Bizseer Technology Company, is an expert in Chaos Engineering. He was invited by CAICT to participate in revising the first domestic Chaos Engineering industry standard in China. He is also the technical core member of AIOps Challenge. His main research interests are AI, including AIOps and Chaos Engineering.

Li Cao is a Master and she is the general manager of the Innovation Business Department in the Beijing BizSeer Technology Company. Her main research interests include AIOps, risk management and Chaos Engineering.

Kanglin Yin is a Ph.D from Tongji University, Shanghai, China and a Postdoctoral fellow in Tsinghua University, Beijing, China. His researches interests include AIOps, software engineering and software system resilence.

Dan Pei is currently an associate professor in the Department of Computer Science and Technology, Tsinghua University. His research interests include network and service management in general. He is an IEEE senior member and an ACM senior member.